The piRNA pathway sustains adult neurogenesis by repressing protein synthesis

One sentence summary: The piRNA pathway is enriched in neural precursors and essential for appropriate neurogenesis by modulating translation

Authors:

Gasperini C.[1], Pelizzoli R.[1], Lo Van A.[1], Mangoni D.[2], Cossu R.M.[2], Pascarella G.[3], Bianchini P.[4], Bielefeld P.[5], Scarpato M.[2], Pons-Espinal M.[1], Sanges R.[2, 6], Diaspro A.[3], Fitzsimons C.P.[5], Carninci P.[4], Gustincich S.[2] and De Pietri Tonelli D[1]§

Affiliations:

1) Neurobiology of miRNA Laboratory, Istituto Italiano di Tecnologia, Genova (Italy)
2) Central RNA Laboratory, Istituto Italiano di Tecnologia, Genova, (Italy)
3) Division of Genomic Technologies, RIKEN Center for Life Science Technologies, Yokohama (Japan)
4) Nanoscopy, CHT Erzelli, Istituto Italiano di Tecnologia, Genoa (Italy)
5) Swammerdam Institute for Life Sciences, Faculty of Science, University of Amsterdam (The Netherlands)
6) Area of Neuroscience, SISSA, Trieste (Italy).

§ Corresponding author, e-mail: davide.depietri@iit.it

Abstract:

In specific niches of the adult mammalian brain, neural progenitor cells (aNPCs) ensure lifelong neurogenesis. Proper regulation of this process entails important implications for brain plasticity and health. We report that Piwil2 (Mili) and PIWI-interacting RNAs (piRNAs) are abundantly expressed in aNPCs but depleted in their progeny in the adult mouse hippocampus. Loss of function of the piRNA pathway in aNPCs inhibited neurogenesis and increased reactive gliogenesis *in vivo* and *in vitro*. PiRNA pathway depletion in cultured aNPCs increased levels of 5S ribosomal RNA, transfer RNAs and mRNAs encoding regulators of translation, resulting in higher polyribosome density and protein synthesis upon differentiation. We propose that the piRNA pathway sustains adult neurogenesis by repressing translation in aNPCs.

In the adult hippocampus, a regulated balance of neural progenitor cells' (aNPCs) quiescence, proliferation and differentiation guarantees lifelong neurogenesis (*1*, *2*), prevents the generation of reactive glia (*3*, *4*), and neurodegeneration (*5*). PIWI-interacting RNAs (piRNAs) are single-stranded noncoding RNAs of 21-35 nucleotides that, in gonads, target transposable elements (TEs) for degradation, thus maintaining germline stem cell pools and fertility (*6*, *7*). In the adult brain, the piRNA pathway was proposed to control synaptic plasticity and memory (*8*–*11*). However, as piRNA levels in neurons are low compared to germline cells (*8*, *9*) and retrotransposition activity increases upon NPC differentiation (*12*), functions of the piRNA pathway in neurons are debated. Interestingly, somatic tissues can reactivate piRNA expression upon oncogenic transformation (*13*) and, apart from gonads, the highest piRNA expression in adult mice has been found in the hippocampus (*14*). Thereby, it is reasonable to hypothesize that in the brain, piRNAs may have a role in aNPCs rather than in neurons.

To this end, we analyzed the expression of Piwil1 (Miwi) and Piwil2 (Mili), essential proteins for piRNA biogenesis and function (*6*, *7*), in aNPCs cultures derived from neural stem cells (NSC) of the adult mouse hippocampus (*15*, *16*) and *in vivo*. As expected, Miwi and Mili proteins were almost undetectable in the whole hippocampus compared to testis (Fig 1A, B). However, the abundance of Mili protein in aNPCs was about 40% of testis (Fig. 1B) and about four folds higher than primary hippocampal neurons (Fig. 1C), in contrast to Miwi protein, which expression was not evident in aNPCs (Fig.1A). To validate this finding *in vivo*, we used a previously published split-Cre viral approach to selectively label NSCs and their progeny in the hippocampus of postnatal Td-Tomato Cre-reporter mice (*16*, *17*). Five days post viral-injection (dpi) in the postnatal hippocampus, we found Mili protein in Td-Tomato positive (Td+) NSCs (Fig. 1D). To quantify Mili expression during neurogenesis, we sorted Td+ NSCs and their differentiated progeny, respectively at 10 and 30 dpi. Expression of *Mili* transcript was higher in Td+ NSCs than in adult-born Td+ neurons (Fig. 1E); the same observation was confirmed at the protein level in cultures of undifferentiated (i.e., proliferating, from here referred to days of differentiation – DIF 0 –) aNPCs and at DIF 4-14 upon induction of neurogenesis (Fig. 1F) with a previously reported viral approach (*18*). These results indicated that Mili is abundantly expressed in neural stem/progenitor cells but depleted in neurons.

To ascertain whether piRNA expression parallels Mili abundance, we extracted and sequenced small RNAs from undifferentiated aNPCs and upon induction of neurogenesis (Fig. 2 A-C). *Bona fide* piRNAs aligned with those previously annotated in the postnatal mouse brain (*19*), had an average length of 30 nt (Fig. 2A) and 5' uridine (U) bias (Fig. 2B). In total, piRNAs clustered in 298 distinct genomic locations (Table S1) and their expression was transient, peaking at the onset of neurogenic differentiation (Fig. 2C, Fig. S1), in agreement with Mili expression pattern during neurogenesis, but not Miwi (Fig. S2A-C). We validated four of the most abundant piRNA clusters in Td+ NSCs sorted from the adult hippocampus, confirming piRNA expression *in vivo* (Fig. 2D). PiR-61648, encoded by one of the piRNA-clusters in our dataset (hereafter referred as piR-cluster 1, Table S1), was recently shown to be selectively expressed in human and murine somatic tissues but depleted in gonads (*20*). Therefore, we extended our analysis to a human NSCs model. PiR-cluster 1 maps on mouse chromosome 8, overlaps with two glycine- transfer RNA (tRNA) loci embedded in an intron of the Vac14 gene and is conserved in human Chromosome 16 (Fig. 2E). Analysis of small RNA datasets from the RIKEN FANTOM5 project (*21*) confirmed the enriched expression of the piR-cluster 1 (Fig 2F) as well as of many other piRNA clusters (Fig. 2G) in human NSCs, compared to differentiated brain cells (Table S2). These results reveal an evolutionary conserved somatic piRNA cluster and indicate that piRNAs are abundantly expressed in neural stem/progenitor cells of both mouse and human.

To infer functions of the piRNA pathway in aNPCs and during neurogenesis, we constitutively knocked-down (KD) Mili by *in vitro* transduction with viruses expressing short-hairpin RNAs targeting *Mili* transcripts, or a scramble short-hairpin RNA as control. Mili KD in undifferentiated aNPCs (Fig. 3A) was sufficient to completely deplete four of the most abundant piRNAs (Fig. 3B). Of note, this manipulation did not affect *Miwi* expression, excluding possible compensatory effects (fig S2 D). Mili loss of function did not alter stemness and proliferation of aNPCs (Fig. S3). However, upon onset of aNPC differentiation it led to their increased survival, likely due to premature cell cycle exit, as apoptosis was unaffected (Fig. S4), and to increased expression of the glial cell marker glial fibrillary acidic protein (GFAP) (Fig. 3C). To inhibit the piRNA pathway *in vivo*, we injected a synthetic oligonucleotide antisense to Mili (GapmeR, MILI KD), or a scrambled GapmeR (Control), in the postnatal mouse hippocampus (Fig. 3D). As early as 48 hours after GapmeR injection, Mili KD (Fig 3E)

led to a dramatic increase in the expression of *Gfap* (Fig. 3E). Inspection of brain sections 30 days after bilateral injections indicated a marked increase of GFAP+ cells with enlarged somas in the ipsilateral hippocampus injected with GapmeR antisense to Mili, compared to cells in the contralateral side injected with control GapmeR (Fig. 3F). To ascertain whether GFAP+ cells were actively generated upon Mili KD, we administered bromodeoxyuridine (BrdU) immediately after GapmeRs injections to label dividing cells in a third cohort of mice (Fig. 3D). 30 days after GapmeRs injection, we found that Mili KD led to a significant increase in adult born GFAP+BrdU+ glial cells at the expense of NeuN+BrdU+ neurons (Fig. 3G).

Increased GFAP expression is generally regarded as a hallmark of astrocyte reactivity and conversion of NSC into reactive glia has been observed in the hippocampus upon ageing or epileptic seizures, at the expense of neurogenesis (*4*, *22*). Indeed, Mili KD increased levels of known reactive glial markers (*22*, *23*) in the postnatal mouse hippocampus (Fig. 3H); and the conversion of NSCs in reactive glia, as induced by Kainic Acid injection in the postnatal mouse hippocampus (*24*), reduced levels of the piRNA pathway in sorted Nestin+ NSCs (Fig. 3I). Altogether, these results demonstrated that Mili is essential for appropriate neurogenesis and suggest that the piRNA pathway mediates reactive gliogenesis in the postnatal mouse hippocampus.

To explore possible mechanisms underlying piRNA pathway functions in neurogenesis, we searched for their putative targets following a previously published pipeline (*19*). Somatic piRNA pathway has been shown to interact with tRNAs (*25*) and other noncoding RNAs, in addition to TEs and mRNAs. In aNPCs, TEs were a minor percentage of the predicted noncoding RNA targets of piRNAs, despite their proportion increased upon induction of neurogenesis (Fig. S5 A, B) in agreement with the observed activation of TEs (*i.e.,* Line1) during neuronal differentiation (*12*, *26*). In contrast, 5S ribosomal RNA (rRNA) and tRNAs were the main predicted piRNA targets in both undifferentiated (47% and 40%, respectively) and differentiating aNPCs (35% and 16%, respectively, Fig. S5 A, B). Analysis of the mRNA targets indicated a prevalence of transcripts encoding proteins involved in ribosome function and protein synthesis (Fig. S5 C), suggesting an involvement of the piRNA pathway in the regulation of translation during neurogenesis. To validate piRNA targets, we quantified their expression in Mili KD aNPCs. PiRNA pathway depletion significantly elevated levels of 5S rRNA and mRNAs encoding for ribosomal proteins and other regulators of translation in both undifferentiated and

differentiating aNPCs (Fig. 4A, B). In contrast, Line1 families of TEs were initially refractory to piRNA depletion and their levels only increased late in differentiation (Fig. S5D). As 5S rRNA, tRNAs and other putative piRNAs targets in aNPCs are essential for ribosome assembly and function, we used stimulated emission depletion (STED) nanoscopy to visualize and quantify polyribosomes (*27*) in aNPCs and in differentiated progeny. Depletion of the piRNA pathway increased polyribosomes in both undifferentiated and differentiating aNPCs, as revealed by immunostaining for the ribosomal protein RPL26, compared to control cells (Fig. 4C, D). However, as the density of ribosomes over transcript does not necessarily correlate with its translation (*28*), we quantified protein synthesis rate by OPP (O-propargyl-puromycin) labelling of nascent proteins during neurogenesis. Indeed, protein synthesis rate was significantly increased upon piRNA pathway depletion in differentiating aNPCs (Fig. 4E, DIF 7). Together, these results support a role for the piRNA pathway in sustaining adult neurogenesis by repressing translation in aNPCs. In agreement, increased translation has been reported to induce differentiation of postnatal NSCs at the expense of self-renewal (*29*).

In summary, we have investigated expression of Mili and Mili-dependent piRNAs in mouse and human NPCs and inferred functions of this pathway in the regulation of neurogenesis in the adult mouse hippocampus. Our data provide the first evidence of an essential role for the piRNA pathway in mammalian neurogenesis. This finding adds a new layer of complexity to the understanding of adult brain plasticity and entails crucial implications for neuronal disorders where dysregulated expression of the piRNA pathway has been reported (*30*, *31*). Our work reveals an unanticipated mechanism of the piRNA pathway in the regulation of protein synthesis. Whereas in germline stem cells Miwi and piRNAs activate translation to sustain spermiogenesis (*32*, *33*), our data suggest that in aNPCs Mili and Mili-dependent piRNAs reduce protein synthesis to sustain neurogenesis. Whereas the possibility that 5S rRNAs, tRNAs (and their fragments), SineB1, here identified as possible piRNA targets, form a coordinated gene-regulatory network regulating translation has yet to be demonstrated, we propose piRNA pathway may be a novel orchestrator of these RNAs in aNPCs.

References

1. J. Altman, *Science.* **135**, 1127–1128 (1962).
2. F. Doetsch, *et al.*, *Cell*. **97**, 703–716 (1999).
3. J. M. Encinas *et al.*, *Cell Stem Cell*. **8**, 566–579 (2011).
4. A. Sierra *et al.*, *Cell Stem Cell*. **16**, 488–503 (2015).
5. T. Toda, *et al.*, *Mol. Psychiatry*. **24,** 67–87 (2019).
6. D. M. Ozata, *et al.*, *Nat. Rev. Genet.* **20**, 89–108 (2019).
7. B. Czech *et al.*, *Annu. Rev. Genet.* **52**, 131–157 (2018).
8. E. J. Lee *et al.*, *Rna*. **17**, 1090–1099 (2011).
9. S. Nandi *et al.*, *Proc. Natl. Acad. Sci. U. S. A.* **113**, 12697–12707 (2016).
10. P. Zhao *et al.*, *Mol. Brain*, 1–12 (2015).
11. L. J. Leighton *et al.*, *Neurobiol. Learn. Mem.* **161**, 202–209 (2019).
12. A. R. Muotri *et al.*, *Nature*. **435**, 903–910 (2005).
13. D. Fagegaltier *et al.*, 1623–1635 (2016).
14. B. P. U. Perera *et al.*, *Epigenetics*. **14**, 504–521 (2019).
15. H. Babu *et al.*, *Front. Neurosci.* **5**, 89 (2011).
16. M. Pons-Espinal *et al.*, *Stem Cell Reports*. **8**, 1046–1061 (2017).
17. R. Beckervordersandforth *et al.*, *Stem Cell Reports*. **2**, 153–162 (2014).
18. S. M. G. Braun, *et al.*, *Stem Cell Reports*. **1**, 114–122 (2013).
19. Y. Ghosheh, *et al.*, *Sci. Rep.* **6**, 25039 (2016).
20. A. G. Torres, *et al.*, *Proc. Natl. Acad. Sci. U. S. A.* **116,** 8451-8456 (2019).
21. D. De Rie *et al.*, *Nat. Biotechnol.* **35**, 872–878 (2017).
22. L. E. Clarke *et al.*, *Proc. Natl. Acad. Sci. U. S. A.* **115**, 1896–1905 (2018).
23. S. A. Liddelow *et al.*, *Nature*. **541**, 481–487 (2017).
24. P. Bielefeld *et al.*, *Front. Neurosci.* **11** (2017).
25. S. P. Keam *et al.*, *Nucleic Acids Res.* **42**, 8984–8995 (2014).

26. N. G. Coufal *et al.*, *Nature*. **460**, 1127–1131 (2009).

27. G. Viero *et al.*, *J. Cell Biol.* **208**, 581–596 (2015).

28. E. W. Mills and R. Green, *Science.* **358** (2017).

29. N. W. Hartman *et al.*, *Cell Rep.* **5**, 433–444 (2013).

30. K. T. Wakisaka, *Front. Biosci.* **24**, 1440–1451 (2019).

31. G. Jain *et al.*, *Transl. Psychiatry*. **9**, 250 (2019).

32. J. Castañeda *et al.*, *EMBO J.* **33**, 1999–2019 (2014).

33. P. Dai *et al.*, *Cell*. **179**, 1566-1581.e16 (2019).

Acknowledgments

We are grateful to G. Hannon (Cambridge, UK) for providing Mili, Miwi antibodies; G. Enikolopov (Stony Brook Univ. NY, USA) for Nestin-GFP mouse. We thank IIT technical staff (S. Bianchi; M. Pesce; E. Albanesi, M. Morini) for excellent assistance. **Funding:** This study was supported by Fondazione Istituto Italiano di Tecnologia; by Fondazione Cariplo Grant #2015-0590 and AIRC-IG 2017 # 20106 to DDPT. P.B. (UvA) and C.P.F. were funded by an ERA-NET-NEURON EJTC 2016 grant and by The Netherlands Organization for Scientific research (NWO). **Author contributions:** Conceptualization: C.G., D.D.P.T; Methodology and experiments: C.G, R.P., D.M., P.B. (UVA), C.P.F., P.B. (IIT), M.S., M.P.E.; *In silico* analysis: A.L.V, R.M.C., G.P.; Data Curation and visualization: C.G.; Writing – original draft preparation: C.G., D.D.P.T; –Editing: all the authors; Supervision: R.S., A.D., C.P.F., P.C., S.G.; D.D.P.T.; Project administration: D.D.P.T.; Funding acquisition: D.D.P.T. **Competing interests:** The authors declare no competing interests. **Data and materials availability:** The mouse small RNA sequencing data have been deposited in the European Nucleotide Archive (ENA) at EMBL-EBI under accession number PRJEB40241; human datasets are available through RIKEN FANTOM5. We apologize to those colleagues whose work could not be cited due to space limitations.

Figure legends

Fig. 1. Hippocampal expression of Mili is enriched in aNPCs and decreases during neurogenesis. (A) Miwi and (B) Mili protein abundance in postnatal mouse testis, hippocampus and undifferentiated aNPCs cultures. (C) Mili protein abundance in cultured mouse hippocampal neurons and aNPCs. (D) Mili (white) expression in Td+ NSC (red) in hippocampal subgranular zone (SGZ); arrows indicate Td+ Mili + cells. (E) *Mili* mRNA expression in sorted Td+ and Td– cells after *in vivo* transduction with split-Cre viruses in the hippocampus. (F) Mili protein abundance in undifferentiated aNPCs (DIF0) and upon induction of neurogenesis (DIF4-14). Data are expressed as mean ± SEM, n = 3 independent experiments. t-Student test or one-way ANOVA Bonferroni as post hoc: *$p < 0.05$, **$p < 0.01$, **** $p < 0.0001$. GCL, granular cell layer; H, Hilus. Scale bars: 10 µm.

Fig. 2. Expression of piRNA clusters during neurogenesis parallels Mili abundance. (A) Size distribution of piRNA reads. (B) Uridine bias at piRNA 5' ends. (C) Mean reads of piRNA clusters in aNPCs (DIF0) and upon induction of neurogenesis (DIF4-7), where the total number of filtered reads in each library ranges between 1,4 - 4,4 x 10^6; Arrows indicate piR-cluster 1. (D) Expression of four of the most abundant piRNA clusters in sorted Td+ and Td- cells 10 dpi of split-Cre viruses in hippocampus. (E) (left) chromosomal location of piR-cluster 1 in mouse and human; (Right) genomic location and sequences (underlined red text) of piR-cluster 1 corresponding to tRNA-Gly genes (underlined black text). (F-G) Expression of piR-cluster 1 (F) and piRNA clusters (G) in human NSC and astrocytes. Data are expressed as mean ± SEM, n = 2 (A-C) and n = 3 (D) independent experiments. t-Student test as post hoc: *$p < 0.05$, **$p < 0.01$.

Fig. 3. The piRNA pathway sustains hippocampal neurogenesis and mediates the generation of reactive glia. (A) *Mili* mRNA (left) and protein (right) levels in aNPCs upon viral transduction of scrambled shRNA (Control) or shRNA targeting *Mili* (Mili KD); western blots of three independent experiments are shown on top). (B) Expression of four of the most abundant piRNA clusters in control and Mili KD aNPCs. (C) *Gfap* mRNA (left) and protein (right) levels in control and Mili KD in differentiating aNPCs (DIF 7). (D) Scheme of the *in vivo* experiment. (E) *Mili* mRNA (left), protein (middle) and *Gfap* mRNA (right) levels in the hippocampus 48

hours after the injection of scrambled (Control) or GapmeR against Mili (Mili KD). (F) Light-microscopy images of postnatal hippocampal sections, immunostained for GFAP, 30 dpi of scrambled (Control, left hemisphere) and GapmeR against Mili (Mili KD, right hemisphere). (G) (Left) Immunostaining for GFAP (green), BrdU (red), NeuN (white) and nuclear DNA (blue) in the hippocampus 30 dpi of scrambled (Control) or GapmeR against Mili (Mili KD); (right) percentages of NeuN+BrdU+ (white arrowheads), or GFAP+BrdU+ (yellow arrowheads) over total BrdU+ cells. (H) mRNA expression of reactive astrocyte markers in the hippocampus 48h upon injection of scrambled (control) or GapmeR against Mili (Mili KD). (I) *Mili* mRNA (left) and piR-cluster 1 (right) expression in sorted GFP+ NSCs from Nestin-GFP mice treated with Saline (Control) or Kainic Acid (KA). Data are expressed as mean ± SEM, n = 3 independent experiments (A-C); n=5 (E); n = 7 (F, G); n = 3 (H, I). t-Student test as post hoc: $*p < 0.05$, $**p < 0.01$, *** $p < 0.001$, **** $p < 0.0001$. Scale bars: 1 mm (F); 100 µm (G).

Fig. 4. PiRNA pathway depletion increases target abundance enhancing polysome assembly and protein synthesis in aNPCs.

(A) expression of SINE B1 and 5S rRNA or (B) mRNAs in undifferentiated (DIF0) and differentiating (DIF4-7) aNPCs upon viral transduction of scrambled shRNA (Control) or shRNA targeting *Mili* (Mili KD). (C, D) Microscopy images (Middle cut: g-STED nanoscopy; Bottom: Confocal; Top: analysis) of control and Mili KD aNPCs (DIF 0 and 7) immunostained for the ribosomal protein RPL26. (Right) normalized distributions of the occupancy, concentration and average of particle size of each polyribosome particle in the indicated cells. (E) Protein synthesis rate (right) as determined by OPP incorporation assay with flow cytometry (left) in control and Mili KD undifferentiated (DIF0) and differentiating (DIF 7) aNPCs. Scale bars: 2 (C); 10 (D) µm. Data are expressed as mean ± SEM, n = 3 independent experiments. t-Student test as post hoc: $*p < 0.05$, $**p < 0.01$.

Fig. 1

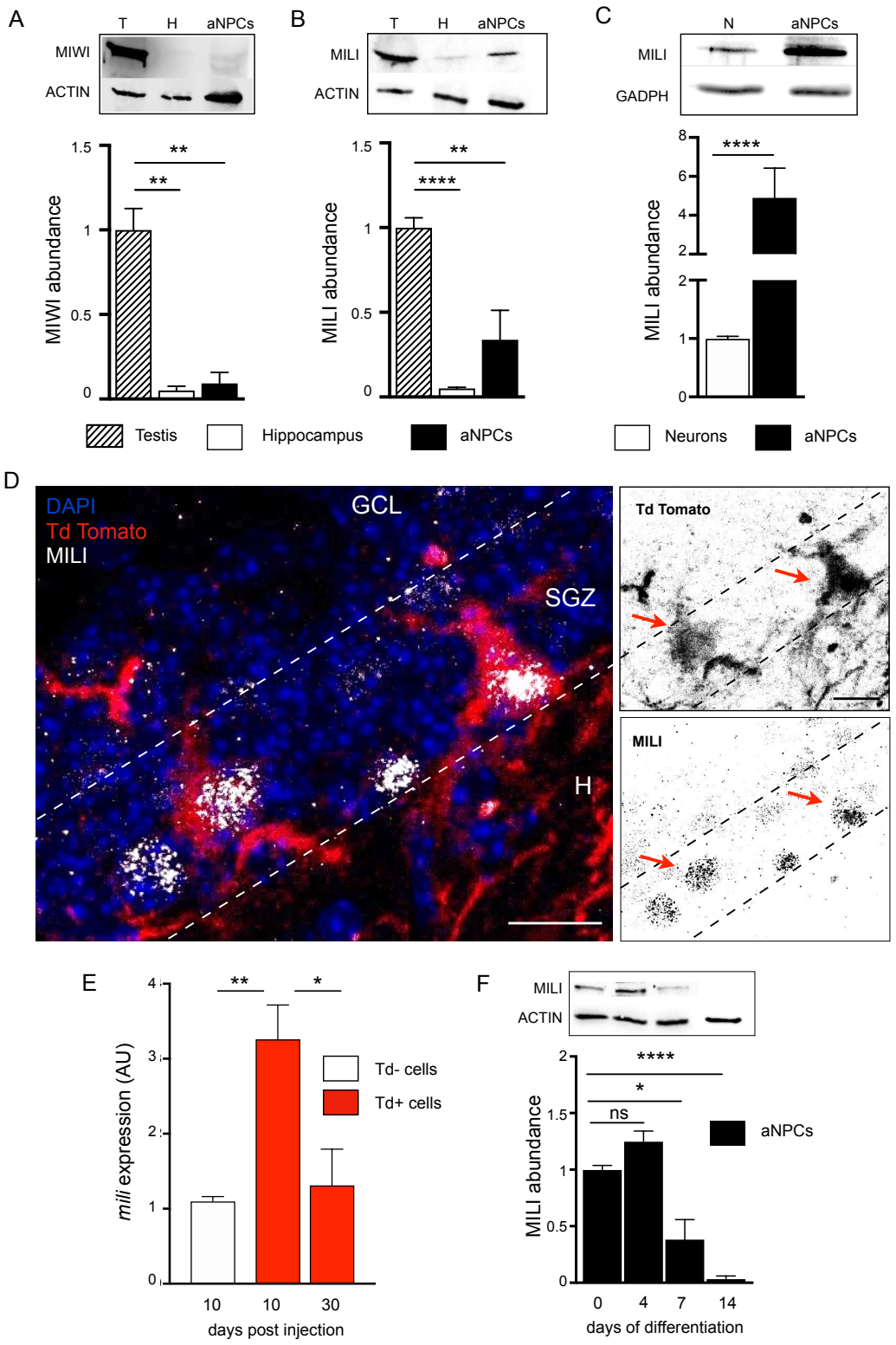
A
T
H
aNPCs
MIWI
ACTIN
MIWI abundance
1.5
1
0.5
0
**
**
Testis
Hippocampus
aNPCs
B
T
H
aNPCs
MILI
ACTIN
MILI abundance
1.5
1
0.5
0
**
****
Hippocampus
aNPCs
C
N
aNPCs
MILI
GADPH
MILI abundance
8
6
4
2
2
1
0
****
Neurons
aNPCs
D
DAPI
Td Tomato
MILI
GCL
SGZ
H
Td Tomato
MILI
E
mili expression (AU)
4
3
2
1
0
**
*
Td- cells
Td+ cells
10
10
30
days post injection
F
MILI
ACTIN
MILI abundance
2
1.5
1
0.5
0
****
*
ns
aNPCs
0
4
7
14
days of differentiation

Fig.2

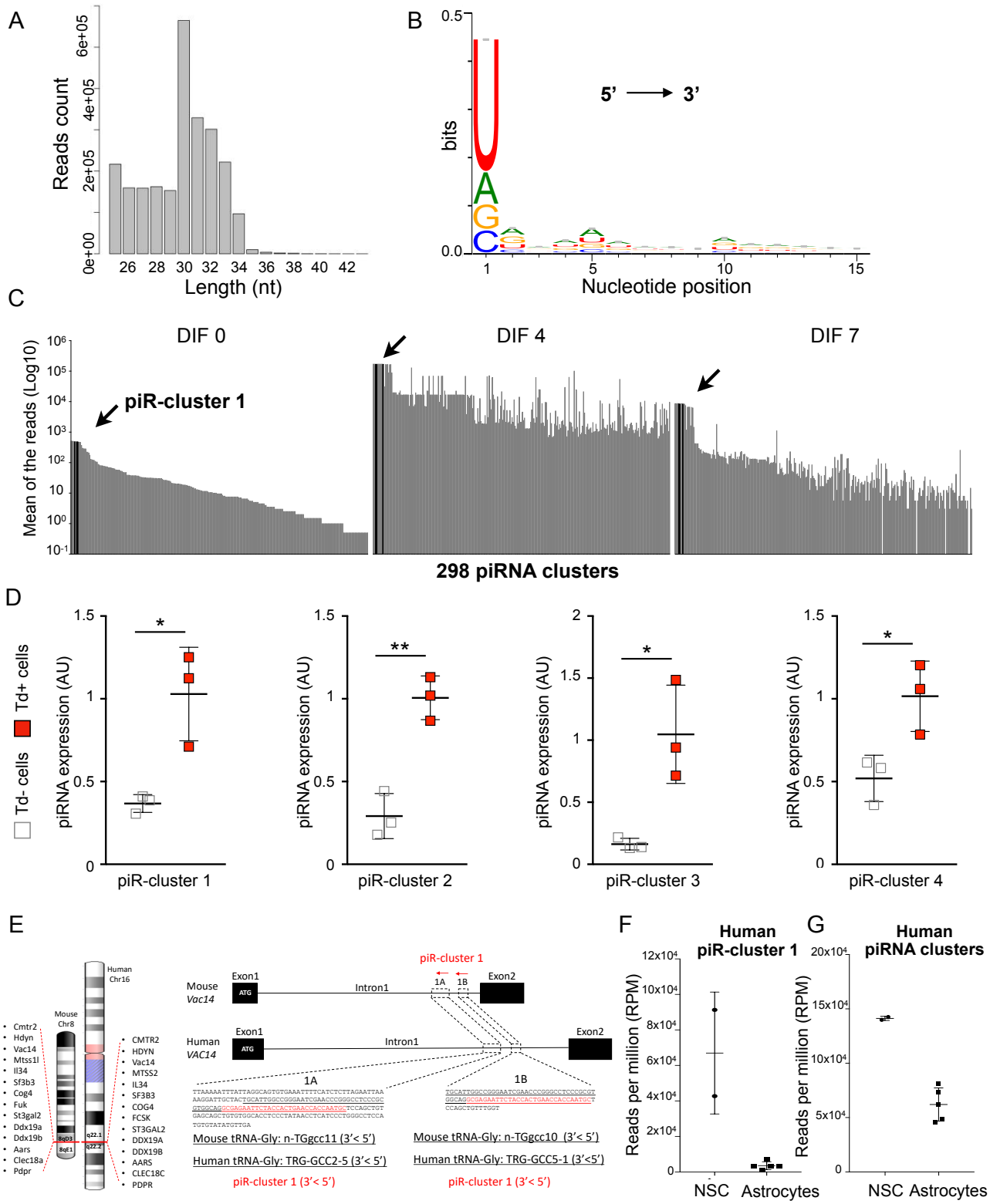
A
Reads count
Length (nt)
B
bits
5' → 3'
Nucleotide position
C
DIF 0
DIF 4
DIF 7
piR-cluster 1
Mean of the reads (Log10)
298 piRNA clusters
D
Td- cells
Td+ cells
piRNA expression (AU)
piR-cluster 1
piR-cluster 2
piR-cluster 3
piR-cluster 4
E
Human Chr16
Mouse Chr8
Mouse Vac14
Human VAC14
Exon1
Intron1
Exon2
piR-cluster 1
1A
1B
Mouse tRNA-Gly: n-TGgcc11 (3'< 5')
Human tRNA-Gly: TRG-GCC2-5 (3'< 5')
piR-cluster 1 (3'< 5')
Mouse tRNA-Gly: n-TGgcc10 (3'< 5')
Human tRNA-Gly: TRG-GCC5-1 (3'<5')
piR-cluster 1 (3'< 5')
F
Human piR-cluster 1
Reads per million (RPM)
NSC
Astrocytes
G
Human piRNA clusters
Reads per million (RPM)
NSC
Astrocytes

Fig. 3

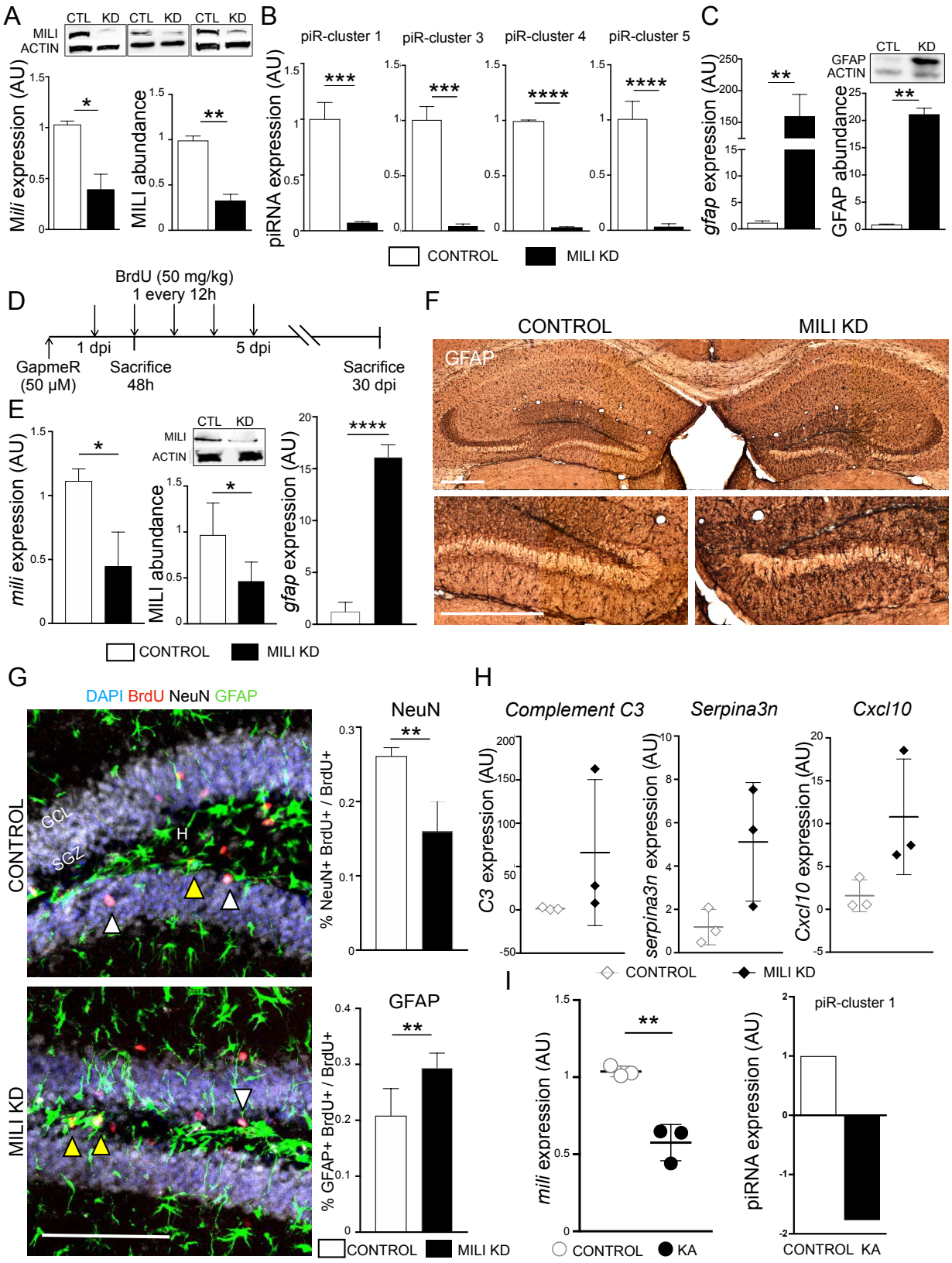
A
CTL KD CTL KD CTL KD
MILI
ACTIN
Mili expression (AU)
MILI abundance
B
piR-cluster 1
piR-cluster 3
piR-cluster 4
piR-cluster 5
piRNA expression (AU)
CONTROL
MILI KD
C
gfap expression (AU)
GFAP ACTIN
GFAP abundance
D
BrdU (50 mg/kg)
1 every 12h
1 dpi
5 dpi
GapmeR (50 µM)
Sacrifice 48h
Sacrifice 30 dpi
E
mili expression (AU)
MILI abundance
gfap expression (AU)
F
CONTROL
MILI KD
GFAP
G
DAPI BrdU NeuN GFAP
CONTROL
MILI KD
GCL
SGZ
H
NeuN
% NeuN+ BrdU+ / BrdU+
GFAP
% GFAP+ BrdU+ / BrdU+
H
Complement C3
Serpina3n
Cxcl10
C3 expression (AU)
serpina3n expression (AU)
Cxcl10 expression (AU)
I
mili expression (AU)
KA
piR-cluster 1
piRNA expression (AU)

Fig. 4

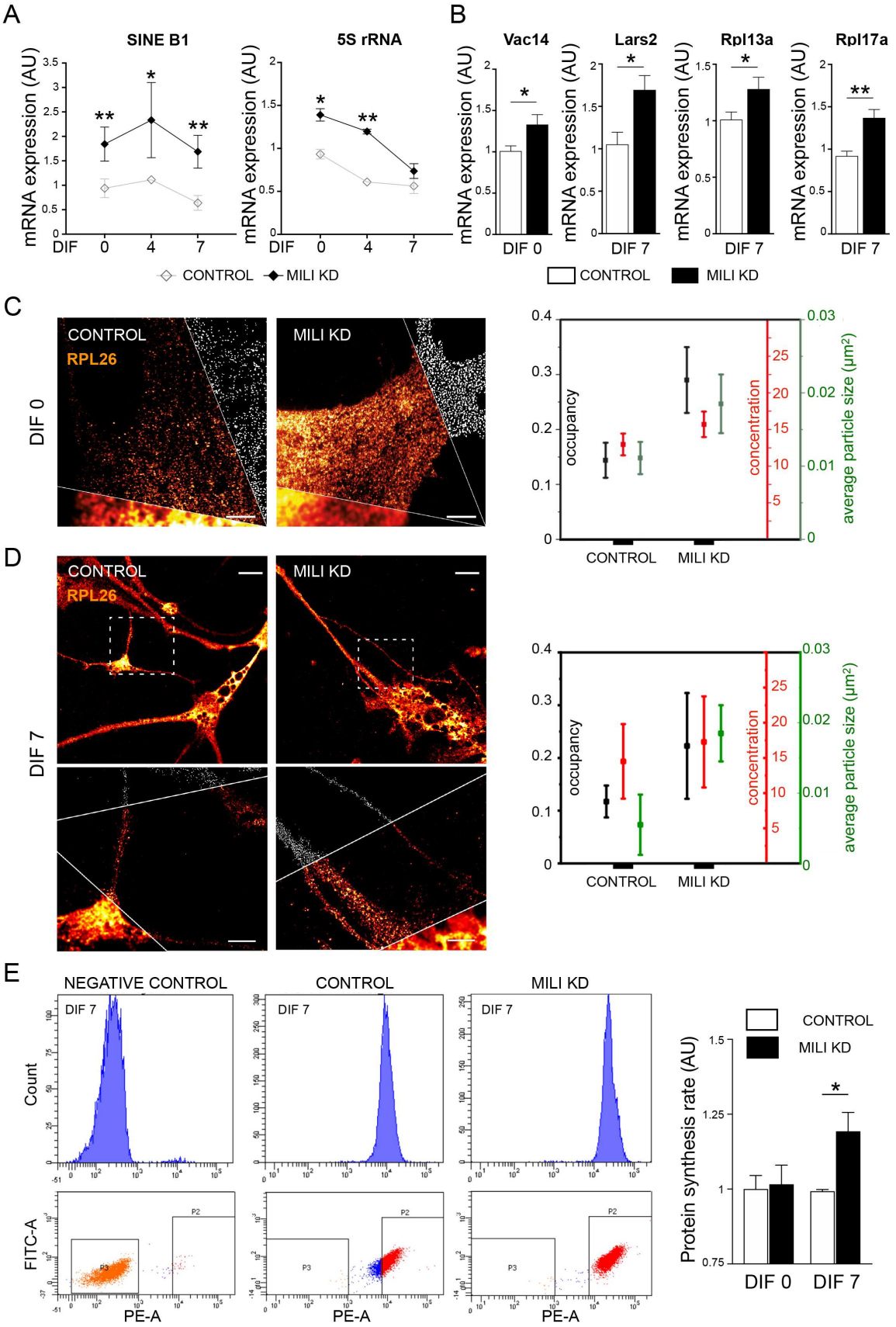
A
SINE B1
5S rRNA
mRNA expression (AU)
DIF 0 4 7
CONTROL
MILI KD
B
Vac14
Lars2
Rpl13a
Rpl17a
DIF 0
DIF 7
C
CONTROL
RPL26
MILI KD
DIF 0
occupancy
concentration
average particle size (μm²)
D
DIF 7
E
NEGATIVE CONTROL
DIF 7
Count
FITC-A
PE-A
P2
P3
Protein synthesis rate (AU)
DIF 0
DIF 7